CRACKING IN NANOSTRUCTURED Li-BATTERIES

K.E. Aifantis[1] & J.P Dempsey[2]
[1]Department of Applied Mathematics and Theoretical Physics, University of Cambridge, UK
[2]Department of Civil and Environmental Engineering, Clarkson University, USA

ABSTRACT

During the charge/discharge cycle of rechargeable Li-batteries, Li-ions are attracted to the negative and positive electrodes interchangeably, and therefore the electrodes expand and contract repeatedly. In order to obtain complete knowledge of rechargeable Li-batteries, the mechanical behavior of the electrodes during each cycle needs to be analysed. A first attempt in this direction was by Aifantis and Hackney [1], who modelled the stress that is developed in the electrodes during the charge/discharge cycle. The most important effect, however, that this Li-insertion/de-insertion has for the electrodes is the formation of cracks, since this affects the electrochemical properties of the battery cell [1]. In the present analysis the geometry considered for both electrodes is that of long cylindrical Li-insertion sites (Sn -- in the negative electrode, and $LiMn_2O_4$ -- in the positive electrode) embedded in a glass matrix. A unit cell consists of a Li-insertion site, whose radius is taken to be 100nm, surrounded by a cylindrical glass area, with radius 1000nm. The cracks that develop at the Sn or $LiMn_2O_4$-glass interface are treated as being radial, in accordance with experimental evidence [1]. By choosing an appropriate displacement condition at the Li-insertion site/glass matrix interface, and by considering three different cases at the glass/glass outer boundary (i.e. stress free surface, clamped surface, self-equilibrated loading) the energy release rate is computed, which allows for the determination of the maximum crack length that can be attained during stable cracking. Sample numerical calculations are presented for the negative electrode.

1 INTRODUCTION

Rechargeable Li-ion batteries have been given considerable attention, due to their unique features. Unlike cadmium and nickel, which are base materials for the widely known nickel-cadmium (Ni-Cd) and nickel-metal-hydride (Ni-MH) batteries, lithium (Li) is non-toxic, and also the third lightest element. In addition, the mass of Li-batteries, due their high energy density is 50% less than that of Ni-Cd or Ni-MH batteries and, thus, the volume required to store them is 20%-50% less. Also, unlike other batteries, Li-batteries do not require an aqueous electrolyte, so they can be used over a wide range of temperatures; this, in combination with the fact that their self-discharge rate is very small over a long period of time, makes them extremely reliable. Finally, one of their most significant properties is a high operating voltage that reduces the number of batteries required to operate a device. As a result, a single Li-battery not only requires less volume for storage, but it can provide three times the voltage of a Ni-Cd or Ni-MH battery. Therefore, not surprisingly, rechargeable Li-ion batteries are the main energy storage devices that are used in the miniaturisation of electronics.

The main topic researchers have focused on in this area is the material selection for the electrodes. The positive electrode (cathode) has to contain Li by definition, since upon charging a voltage is applied between the two electrodes, i.e. electrons flow into the negative electrode (anode), and thus Li-ions diffuse from the cathode to the anode; the opposite occurs during discharge. The capability of the electrode materials to store Li-ions plays a detrimental role in the capacity of the battery.

As mentioned earlier since the cathode must contain Li, it has traditionally been comprised of glass or ceramic and a Li-compound, which acts as the Li-insertion site. The materials, however, that have been used for the anode have been replaced over the years, and research is still being conducted for the most optimum selection. Until 1980 Li metals and alloys were used as anode materials but due to safety problems that resulted from this material selection, carbon-based Li-ion intercalation materials were solely used as the anode material after 1985. As a result, the capacity of the batteries has been limited by the Li-storage capacity of carbon materials, which is confined by the stoichiometric limit of Li-ion intercalation in graphite (LiC_6). This limit can be exceeded but after continuous electrochemical cycling the Li-batteries tend to form hazardous metallic Li dendrites on the electrode surface, rendering them commercially unusable for safety reasons. An alternative configuration that has been proposed, recently, for the anode is one that is essentially the same as that of the cathode, i.e. a compound that acts as a host for the Li-ions in combination with a glass or ceramic. The main difference then, between the two electrodes is the compound (active material) that is used as the Li-insertion site. In the cathode it is a chemical compound of Li, such as lithium cobalite ($LiCoO_2$), lithium nickelite ($LiNiO_2$), or lithium manganese oxide spinel ($LiMn_2O_4$) embedded in a glass matrix.

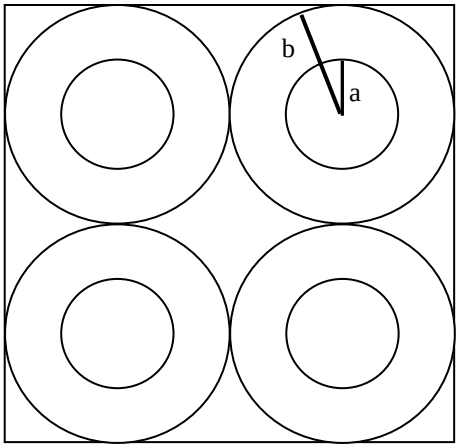

Figure 1: Geometry of electrodes: Li-insertion particles (of radius *a*) embedded in a glass matrix. A unit cell is defined by a glass area of radius *b* surrounding a $LiMn_2O_4$ or Sn inclusion of radius *a* (see also Figure 3).

Whereas in the anode it can be active "sphere-like" Si particles encased in inactive ion conducting tin matrix, or Sn particles surrounded by Fe_3C (or $SnOLiOP_2O_5$) ceramic matrix. High Li-capacity templated anodes consisting of about 100nm SnO_2 nanofibers have also been used. The electrode configurations that will be used for the present study will be that according to which both the cathode and anode consist of Li-insertion material and glass. The active material in the cathode will be taken to be $LiMn_2O_4$ and for the anode Sn. The geometry assumed is that of long cylindrical Li-active sites, of radius *a* embedded periodically in a glass matrix; the area that surrounds each active site is also taken to be cylindrical of radius *b* (Figure 1). Since the only difference between the electrodes is the Li-insertion material the analysis that follows is valid for both the anode and cathode; numerical results, however, are obtained only for the anode.

2 CRACKING IN Li BATTERIES

It has been observed experimentally that during continuous electrochemical loading (which occurs during the charge/discharge cycle), the active site/glass matrix interface fractures. This is of great importance because the fracturing of individual particles is believed to degrade the electrochemical properties of the electrode. This occurs because the active material which fractures is no longer in electrical contact with the remainder of the electrode and is therefore unable to respond to the applied voltages necessary to recharge or control the discharge of the battery. In addition, corrosive agents, such as HF and residual H_2O, which are present in the battery, are believed to attack the surfaces of the active material and the fracture of individual particles results in an increase of the surface area available to this chemical attack. In fact, it is reasonable to expect that the chemical instability of the active particle surfaces may interact to enhance the structural instability (stress corrosion cracking).

Electrochemical cycling experiments that were performed at Michigan Tech [1] on a single $LiMn_2O_4$ crystal showed that the outer surface fractured in the manner depicted in Figure 2. It can thus be assumed that around each active site in the electrodes (in the annular region enclosed by the radii *a* and *b*), a fracture layer such as that in Figure 2 will form. By reference again to the same figure it can be deduced that a realistic model of this fracture layer could assume radial crack growth. According to this approach the unit cell is modelled as in Figure 3. As mentioned earlier, *a* and *b* are the radii of the active Li-insertion site and surrounding glass, respectively. The stress the Li-ions exert onto the active site is taken to be uniform, according to [1], and equal to a constant *p*. Due to this pressure *p*, the active site would expand a distance Δ, in the absence of the glass matrix. The pressure at the glass/glass interface (at the outer boundary of the unit cell) is taken to be *q*. Finally, the length of the cracks that would initiate and propagate by the continuous charge/discharge cycle is symbolised by ρ.

For the numerical calculations the Li-insertion particle will be taken to be Sn, and the glass matrix, will be taken to be soda glass. Therefore the elastic modulus (*E*) and Poisson's ratio (*v*) will be 41GPa and 0.33 for

the Sn, while for the soda glass they will be 75GPa and 0.23. The geometric parameters will be a=100nm, b=1000nm and Δ=145nm. The reasoning behind the computation of Δ is provided by Aifantis [1].

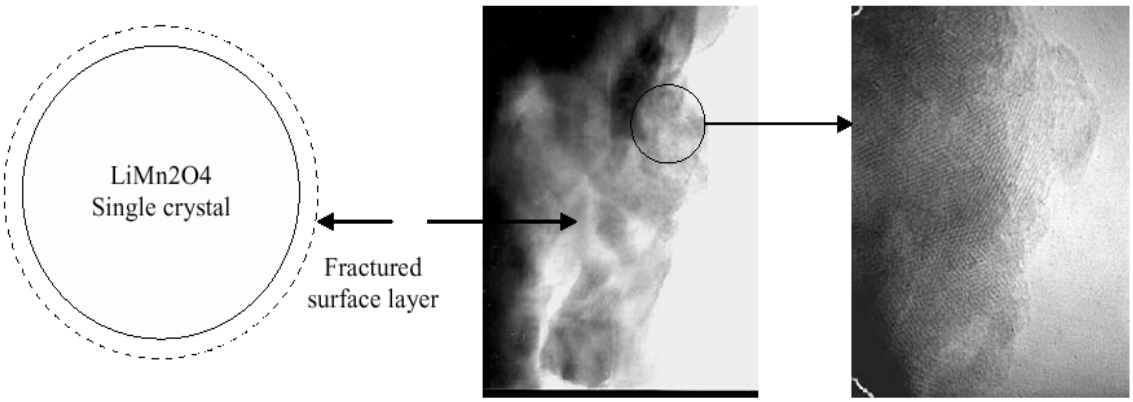

Figure 2: Deep discharged $LiMn_2O_4$ particles with associated fractured surface layers. Chemo-mechanical stresses develop as a result of Li insertion and de-insertion.

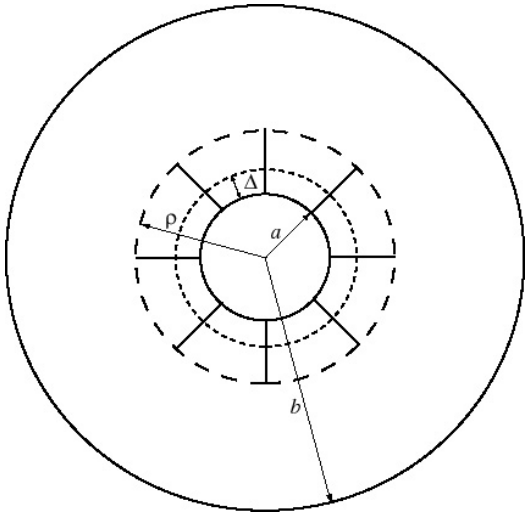

Figure 3: Unit cell under consideration

3 DISPLACEMENT AND STRESS EXPRESIONS IN UNIT CELL

Due to the assumption that the Li-insertion sites are long cylinders, conditions of plane strain in polar co-ordinates will be assumed in the analysis that follows.

As in [1] prior to the formation of cracks the stresses and displacements inside the active site and glass, can be solved, by consideration of appropriate boundary conditions from the common Lamé equations, which state that

$$\sigma_{rr}(r)=\frac{A}{r^2}+2C, \text{ and }, \; u_r(r)=\frac{1}{E}\left[\frac{-A(1+\nu)}{r}+2C(1-2\nu)(1+\nu)r\right] \quad (1)$$

where A and C are constants. According to the reasoning in the previous section it is easy to deduce that the stresses at the interfaces at $r = a$ and $r = b$ are given by

$$\sigma_{rr}(a)=-p,\sigma_{rr}(b)=-q,\sigma_{r\theta}(a)=\sigma_{r\theta}(b)=0\,. \quad (2)$$

Now we deduce an appropriate displacement condition at the Li-active site/glass interface, as follows. Since the stress the Li-ions exert onto the active site is constant, it is independent of the radial distance r, and therefore A=0 for all expressions in eqn(1) for the active site. Also as it was mentioned previously if

the active site was unconfined it would reach a radius of $a+\Delta$, during maximum Li-insertion. Under confined conditions, though, the actual expansion is decreased by the pressure p being applied by the outer ceramic, by the amount

$$u_r(a+\Delta) = -\frac{p(1-2v_s)(1+v_s)(a+\Delta)}{E_s}, \tag{3}$$

where from now on the material constants inside the Li-insertion site will have subscripts s (when refering to the glass no subscripts will be used). Therefore, given the present configuration, the displacement at the active site/glass interface is given by

$$u_r(a) = \Delta - \frac{p(1-2v_s)(1+v_s)(a+\Delta)}{E_s} \quad . \tag{4}$$

After continuous electrochemical cycling radial cracks initiate at this active site/glass matrix interface. Therefore stress and displacement expressions that govern behavior in this damage zone need to be formulated. The formulation is similar to that done by Dempsey et al [2]. Within the cracked region a uniaxial state of stress is assumed to exist, thus $\sigma_{\theta\theta} = \sigma_{r\theta} = 0$, while equilibrium conditions along the radial direction require that

$$\frac{d\sigma_{rr}}{dr} + \frac{\sigma_{rr}}{r} = 0 \Rightarrow \sigma_{rr}(r) = \frac{k}{r}, \text{ for } a \le r \le \rho \tag{5}$$

where k is a constant. Given that $\sigma_{rr}(a) = -p$, it follows that $k = -pa$. Furthermore, under plane strain conditions, there is no strain in the z-direction and so

$$\sigma_{rr} = E'\frac{du_r}{dr} \Rightarrow \frac{du_r}{dr} = \frac{-pa}{E'r} \Rightarrow u_r(r) = -\frac{pa}{E'}\ln(r) + u^*, \text{ for } a \le r \le \rho \tag{6}$$

where $E' = E/(1-v^2)$ and the constant u^* can be found by setting the displacement right in front of the crack tip (which is inside the uncracked region) equal to $u_+(\rho)$ and then subtituting back into eqn(6), i.e.

$$u_r(\rho) = u_+(\rho) \Rightarrow u_+(\rho) = -\frac{pa}{E'}\ln(\rho) + u^* \Rightarrow u^* = \frac{pa}{E'}\ln(\rho) + u_+(\rho). \tag{7}$$

It should be noted that $u_+(r)$ will be defined next. Inserting eqn(7) in eqn(6) we can conclude that inside the cracked region the radial displacement is given by

$$u_r(r) = \frac{pa}{E'}\ln\left(\frac{\rho}{r}\right) + u_+(\rho), \text{ for } a \le r \le \rho. \tag{8}$$

Now the last region that needs to be modelled is the uncracked region that lies between the radial crack tip boundary and the glass/glass interface. This area can be treated as a hollow cylinder that is subject to an internal pressure p_*, which is exerted by the Li-active site inclusion, and an external pressure q, that is exerted from the neighbouring unit cell. The internal pressure is equal to that present at the interface with the fractured region (i.e. at $r = \rho$) and it can be found by direct substitution in eqn(5), i.e.

$$p_* = -\sigma_{rr}(\rho) = pa/\rho. \tag{9}$$

The displacement expression valid for such a hollow cylinder, i.e. that is subjected to an internal and external pressure, has been solved by Westergaard [3], and reads

$$u_+(r) = \frac{r}{2\mu}\left\{p_*\frac{b^2/r^2 + (1-2v)}{b^2/\rho^2 - 1} - q\frac{\rho^2/r^2 + (1-2v)}{1-\rho^2/b^2}\right\} \text{ for } \rho \le r \le b, \tag{10}$$

where the constant $\mu = E/(2+2v)$.

Thus by inserting eqn(10) into eqn(8), a second expression for the displacement at $r = a$ can be deduced as

$$u_r(a) = \frac{pa}{E'}\left\{\ln\left(\frac{\rho}{a}\right) + 2\frac{b^2 - Cb\rho}{b^2 - \rho^2} - \frac{1-2v}{1-v}\right\}, \tag{11a}$$

where $C = qb/pa$. Moreover, the displacement at $r = b$ can also be deduced, from eqn(10) as

$$u_r(b) = \frac{pa}{E'}\left\{2\frac{b\rho - Cb^2}{b^2 - \rho^2} + \frac{C}{1-v}\right\}. \tag{11b}$$

4 STABILITY INDEX FORMULATION

As mentioned in the introduction the purpose of this work is to model crack growth in Li-batteries. This can be accomplished by examining the behaviour of the stability index. To do this, one first needs to define an expression for the energy release rate, *G*. Dempsey et al [4] determined that *G* may be expressed as

$$G(\rho)=\frac{\pi\rho}{E'n}\sigma_{\theta\theta}^{2}(\rho^{+}), \tag{12}$$

where *n* is the number of radial cracks, and $\sigma_{\theta\theta}(\rho^{+})$ can be deduced from [3] as

$$\sigma_{\theta\theta}(\rho^{+})=\frac{pa}{b}\left\{\frac{1+(\rho/b)[(\rho/b)-2C]}{(\rho/b)[1-(\rho/b)^{2}]}\right\}. \tag{13}$$

Now the stability index can be defined as

$$\kappa=\frac{b}{G}\frac{dG}{d\rho}. \tag{14}$$

The energy release rate depends on the material parameters (*E*, *v*), the geometric parameters (*a*, *b*), the number of cracks *n*, and the internal and external pressures *p* and *q*. The internal pressure can be found by equating expressions eqn(4) and eqn(11a), and solving for *p*, while the external pressure *q* need not be defined explicitly as long as *C* is. Below are solutions to three different cases:

4.1 Case 1: Traction Free Outer Boundary

In the first case that will be examined the outer pressure is taken to be zero, i.e. the stress exerted by the Li-insertion site on the glass is fading away with increasing distance and becomes vanishingly small at the outer cell boundary. Therefore, *q*=0, which implies that *C*=0, and by equating eqn(11a), which of course has simplified with, eqn(4) the internal pressure can be found as a function of the geometric and material parameters. Inserting the resulting expression in eqn(13), along with the fact that *C*=0, one can obtain the energy release rate for this case, G_1, as:

$$G_1(\rho)=\frac{\pi p_1^{\,2}a^{2}}{nE'\rho}\left\{\frac{b^{2}+\rho^{2}}{b^{2}-\rho^{2}}\right\}^{2},\ \text{where}\ \ p_1=\Delta\left\{\frac{a}{E'}\left[\ln\left(\frac{\rho}{a}\right)+2\frac{b^{2}}{b^{2}-\rho^{2}}-\frac{1-2v}{1-v}\right]+\frac{(a+\Delta)}{\Gamma}\right\}^{-1}. \tag{15}$$

It should be noted that $\Gamma=\dfrac{E_s}{(1-2v_s)(1+v_s)}$.

4.2 Case 2: Clamped Outer Boundary

The second case that is physically possible for the configuration under consideration, is that the displacement at the glass/glass interface is zero, i.e. the force the unit cells exert onto one another is equal and opposite and therefore the displacements at this boundary annhilate each other out. Therefore *u*(*b*)=0, and by setting eqn(11b) equal to zero, one can solve for *C* to obtain:

$$C=\frac{2(1-v)b\rho}{(1-2v)b^{2}+\rho^{2}}. \tag{16}$$

By inserting eqn(16) in eqn(11a), and setting it equal to eq(4), similarly as before, the internal pressure can be found. Therefore the energy release rate for this case, G_2, reads

$$G_2(\rho)=\frac{\pi p_2^{\,2}a^{2}}{nE'\rho}\left\{\frac{(1-2v)b^{2}-\rho^{2}}{(1-2v)b^{2}+\rho^{2}}\right\}^{2} \tag{17}$$

where

$$p_2=\Delta\left\{\frac{a}{E'}\left[\ln\left(\frac{\rho}{a}\right)+2\frac{(1-2v)b^{2}}{(1-2v)b^{2}+\rho^{2}}-\frac{1-2v}{1-v}\right]+\frac{(a+\Delta)}{\Gamma}\right\}^{-1}. \tag{18}$$

4.3 Case 3: Self-Equilibrated Loading

The final case that is considered, which seems to be the most probable, is that of self-equilibrated loading, i.e. the force (*qb*) that is exerted on the outer glass annulus by a surrounding unit cell is equal to the that

exerted onto it by the Li-insertion site (*pa*). Therefore *C*=1, and by solving for the internal pressure (by equating eqn(4) and eqn(11a)), the energy release rate is obtained as

$$G_3(\rho)=\frac{\pi {p_3}^2 a^2}{nE'\rho}\left\{\frac{b-\rho}{b+\rho}\right\}^2 \text{, where } \quad p_3=\Delta\left\{\frac{a}{E'}\left[\ln\left(\frac{\rho}{a}\right)+2\frac{b}{b+\rho}-\frac{1-2\nu}{1-\nu}\right]+\frac{(a+\Delta)}{\Gamma}\right\}^{-1}. \tag{19}$$

Now the stability index, κ, can be defined for each case, and by taking the same material and geometric parameters as in [1], and setting the number of radial cracks (*n*) equal to five, one obtains the following stability plot (Figure 4). Stable crack growth is likely to occur for negative values of κ and therefore the crack length at which the x-axis is crossed indicates the maximum distance a crack can propagate under stable conditions. It can be seen from Figure 4 that for case 1 the maximum stable crack length is attained at a very small distance and for case 2 an asymptote is observed.
Therefore case 3 is physically the most probable since it suggests stable crack growth until the outer radius *b* is reached.

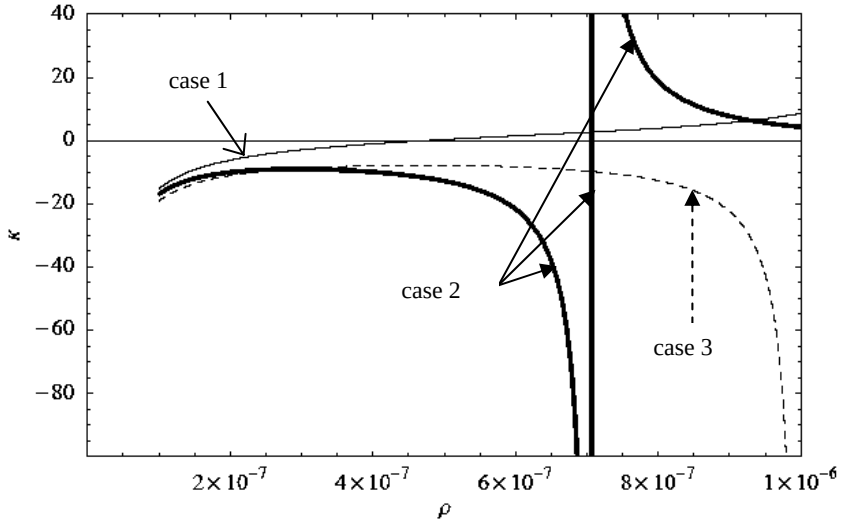

Figure 4: Crack growth stability in the anode of Li batteries (crack length ρ in meters)

References:
[1]Aifantis KE, Hackney SA, An ideal elasticity problem for Li-batteries J. Mech Behavior of Matls, (to appear)
[2]Dempsey JP, Palmer AC, Sodhi DS, High pressure zone formation during compressive ice failure, Eng. Fract. Mech., 68, 1961-1974, 2001
[3]Westergaard HM, Theory of Elasticity and Plasticity, Harvard University Press, 1952
[4]DempseyJP, Slepyan LI, Shekhtman II, Radial cracking with closure, Int. J. Fract, 73, 233-261, 1995